

Longterm Late-Wood ^{13}C signatures in Iberian *Pinus pinaster* Ait. induced by climate

W. Lara^{a,c,1,*}, C. Ordoñez^a, F. Bravo^a, C. A. Sierra^a

^aSustainable Forest Management Research Institute, UVA-INIA, Avenida Madrid, s/n,
34071, Palencia, Spain

^bDepartment of Biogeochemical Processes, Max Planck Institute for Biogeochemistry,
Hans-Knöll-Straße 10, 07745, Jena, Germany

^cResearch Center on Ecosystems and Global Change, Carbono & Bosques (C&B), Calle
51A, No 72-23, Int: 601, 050034, Medellín, Colombia

Abstract

Keywords:

¹ **1. Introduction**

² This study aims to study long-term effects of drought on tree growth and
³ isotopic discrimination of *P. pinaster* in north and east-central Spain.

*Corresponding author

¹E-mail address: wilson.lara@alumnos.uva.es (W.Lara)

⁴ This is the introduction

5 **2. Materials and Methods**

6 *2.1. Study area*

7 We developed our study in two areas in east Spain and north-central Spain
8 (Fig. 2). The areas belong to the most vast native provenance region of mar-
9 itime pine (*Pinus pinaster* Ait.) forests, growing on sandy soils (Inceptisols and
10 Aridisols) forming large continuous populations at moderate densities (average
11 of 500 - 1000 trees per hectare). Forest ecosystems of the area are associated
12 with oaks (*Quercus ilex* L., *Q. faginea* Lam., and *Q. pyrenaica* Willd.), beeches
13 (*Fagus silvatica* L.), and other pine species (*Pinus sylvestris* L., *P. nigra* Arn.
14 and *P. halepensis* Mill). Average altitude for this region ranges from 900 m to
15 1000 m above sea level. The forests are influenced by Mediterranean climate
16 with dry and warm summers and cool to mild winters. Mean annual tempera-
17 ture is about 11 °C and mean annual precipitation is approx. 562 mm.

18 *2.2. Core sampling*

19 Dominant trees of maritime pine growing in ten locations in the study site
20 where core sampled (5 mm diameter) at chest height (1.3 m). These were
21 located in five locations of north-central edge of the study site and the other
22 five locations were established on the eastern edge. Two dominant trees were
23 sampled by site, and two core samples were extracted from each tree. The core
24 samples were air dried, sanded, and scanned (1000:1600 ppi). Tree-ring Widths
25 (TRWs) in the scanned images were measured and statistically controlled with
26 R-packages `measuRing` (Lara et al., 2015) and `dplR` (Bunn, 2010), respectively.

27 A master chronology of 150 trees of *P. pinaster* for the study area (Bogino
28 and Bravo, 2008) was used to develop the statistical control of the TRW. The
29 chronology has strong common signal (EPS > 0.95, SNR > 22). The cross-
30 dating process was controlled by grouping the data in four common regions,
31 which were defined after clustering the tree-dimensional coordinates of the sam-
32 pling locations, with each of the clusters having sites at most 80 km of closeness
33 (Figure 1).

34 2.3. *climatic data*

35 We processed a high-resolution gridded dataset (0.11° resol.) of monthly
36 cummulative precipitations and monthly mean temperatures for peninsular Spain
37 (Herrera et al., 2015, Spain02) across Ebro basin (1971 - 2010). Proyection of
38 UTM coordinates of the sample plots to coordinate system in climate algorithm
39 was developed with R-package `rgdal` (Bivand et al., 2015). After projecting the
40 gridded dataset, meteorological series corresponding to coordinates of sample lo-
41 cations were extracted. These were used to compute **Standardized Precipitation**
42 **Indexes (SPI)** extracted with R-packages `raster` (Hijmans, 2015) and `SPI`.

43 2.4. *Late-Wood Stable $\delta^{13}\text{C}$*

44 One core replicate per sample location was processed for **Late-Wood Stable**
45 **$\delta^{13}\text{C}$ (LWSC)** analysis. Late wood in radial increments of the cores were care-
46 fully separated from the earlywood with a microtome. Only rings that were
47 formed after 1974 were analysed. Whole wood was milled, an aliquot of 100 mg
48 was packed in porous bags and used for cellulose extraction. The samples were
49 washed in 5 percent NaOH solution twice for 2 h at 60°C in order to remove
50 fats, oils, resins and hemicellulose. In a second step the lignin was removed with
51 NaClO 2.7% After each treatment the samples were washed with distilled water
52 and then finally dried overnight at 60°C .

53 The $\delta^{13}\text{C}$ was determined using an elemental analyser linked to an isotopic
54 ratio mass spectrometer via a variable open split interface (Max Plank Institute
55 for Biogeochemistry, Germany). The results of laboratory were presented in the
56 δ notation:

$$\delta = [(R_{sample}/R_{standard}) - 1] \times 10^3 \quad (1)$$

57 relative to the internationsl VPDB standard for cabon; where R_{sample} and
58 $R_{standard}$ is the fractions of $^{13}\text{C}/^{12}\text{C}$ for the sample and the standard, respec-
59 tively. The standard deviation for the repeated analysis (commercial cellulose)
60 was better than 0.1. was better than 0.1 percent. The calibration versus VPDB

61 was done by measuring IAEA USGS-24(graphite) and IAEA-CH7 (polyethylene).
62

63 *2.5. Inter-annual relationships*

Signals in annual late-wood $\delta^{13}\text{C}$ and annual aridity index were compared with wavelet coherency (Cazelles et al., 2008). This time-series comparison method produces cross-correlation contour plots between periods of the signals and the time. Colors of the contour plots vary from blue to red and illustrate correlations values from zero (absent signal correlation) to one (maximum signal correlation), respectively (Fig. 6). Wavelet coherency is based on the theory that signals can be decomposed over mother wavelets $\varphi(t)$. These are expressed as function of two parameters: the time position (τ), and the scale of the wavelets (a):

$$\varphi(t) = \left(\frac{t - \tau}{a} \right). \quad (2)$$

The wavelet coherency is computed following three steps. First, wavelet transform of each time series is calculated. For example, the wavelet transform of the late-wood $\delta^{13}\text{C}$ time series $\delta(t)$ is calculated as follows:

$$W_x(a, \tau) = \frac{1}{\sqrt{a}} \int_{-\infty}^{\infty} \delta(t) \varphi^* \left(\frac{t - \tau}{a} \right) \quad (3)$$

64 were $W_x(a, \tau)$ are wavelet coefficients representing contribution of scales (a)
65 to the signal at different time positions (τ). The * sign denotes the complex
66 conjugate form.

67 This procedure produces normalized cross-spectrums comparing time-scales
68 and localizations of the time series. Cross-spectrums are level plots of cross-
69 correlations between time series

The wavelet coherence is defined as the cross-spectrum normalized by the spectrum of each signal.

$$W_{x,y}(f, \tau) = W_x(f, \tau) W_y(f, \tau) \quad (4)$$

70 We compared the series of annual late-wood $\delta^{13}\text{C}$ and annual aridity index
71 with wavelet coherency (). This approach enables comparison of properties of
72 two time series principally its time-scale and localization.

73 The wavelet cross-spectrums are correlograms

74 The wavelet cross-spectrums is defined as follows:

75 where $W_x(f, \tau)$

76 3. Results

77 3.1. Tree-growth fluctuations

78 Patterns in **TRW** fluctuations were more regular in locations of east Spain
79 than in locations of north-central Spain regardless trends in **TRW** chronologies
80 were or were not subtracted.

81 In locations of east Spain, smoothing spline over time of original **TRW**
82 chronology exhibited regular sinusoidal patterns (Fig. 3, lower-left panel).
83 Lower extremes of the spline were observed during the decade starting in 1990
84 and higher extremes of the spline were evidenced during the decades starting in
85 1970 and 2010. The smooting spline over time in the detrended **TRW** chronol-
86 ogy illustrated similar sinusoidal patterns with regard to the patterns observed
87 in the original **TRW** chronology (Fig. 3, lower-right panel).

88 In locations of north-central Spain, the smooting spline over time of original
89 **TRW** chronology indicated a decreasing exponential pattern (Fig. 3, upper-left
90 panel). Higher extremes of this curve were evidenced in the decade starting in
91 1979 and lower extremes were observed in the decade starting in 2010. The
92 spline of the corresponding detrended chronology was sinusoidal with higher
93 extremes observed in the decades of 1970 and 2000, and the lower extremes
94 observed in the decades starting in 1990 (Fig. 3, upper-right panel).

95 3.2. Late-Wood Stable $\delta^{13}\text{C}$ fluctuations

96 In contrast to the tree-growth fluctuations, patterns in **Late-Wood Stable**
97 $\delta^{13}\text{C}$ (**LWSC**) fluctuations were more regular in detrended chronologies than in
98 original chronologies regardless the ubication of the sampling locations.

99 In locations of east Spain, the spline over time in original **LWSC** chronology
100 followed an irregular and decreasing sinusoidal pattern (Fig. 4, lower-left panel)
101 with the maximum extreme of the spline being evidenced during the decade
102 starting in 1980, followed by a pulse with minimum and maximum relatives
103 occurring during the decade of 1990, and ending with lower extremes in the
104 decade starting in 2010. Spline of corresponding detrended **LWSC** chronology
105 (Fig. 4, lower-right panel) indicated more regular sinusoidal pattern to that
106 observed in the original chronology. This curve had decadal pulses with maximal
107 extremes occurring around 1980, 1990, and 2005.

108 In locations of north Spain, the spline of the original **LWSC** chronology de-
109 picted irregular and decreasing sinusoidal pattern (Fig. 4, upper-left panel)
110 with spline oscillations slowing during second half of 1980 and a minimum ex-
111 treme occurring around 2005. Spline of detrended **LWSC** chronology illustrated
112 more regular sinusoidal pattern regard the curve of original chronology (Fig. 4,
113 upper-right panel) with similar slowing oscillation around second half of 1980
114 and minimal relatives occurring around 1975, 1995, and 2010.

115 *3.3. Intra-annual response coefficients*

116 Responses of **TRW** to monthly climatic fluctuations were similar in both
117 north-central Spain and east Spain (Fig. 5). The tree-growth chronology was
118 correlated with precipitation regimes of the winter season and uncorrelated with
119 precipitations of the other seasons. The significant correlations between tree
120 growth and winter precipitation were slightly stronger in eastern than in north-
121 central edges of study site and occurred within a month of each other: i.e.
122 January in north-central Spain and February in the west. No conclusive rela-
123 tionships between tree growth and seasonal temperature were observed along the
124 study site.

125 On the other hand, responses of **LWSC** to the monthly fluctuations were dif-
126 ferent in the locations. In north central Spain, the **LWSC** significantly responded
127 to summer temperatures and no significant correlations were evidenced between
128 the stable isotope and the temperature in the other seasons. No conclusive re-

¹²⁹ lationships responses between **LWSC** and temperature were evidenced. In east
¹³⁰ Spain, the **LWSC** significantly responded to spring precipitations while no sig-
¹³¹ nificant responses were observed in other seasons. No conclusive relationships
¹³² between tree growth and seasonal temperatures were observed along the study
¹³³ site.

¹³⁴ *3.4. Wavelet coherency*

¹³⁵ Relationships between tree growth and drought fluctuations depended on
¹³⁶ sampling locations (Fig. 6). The tree-growth fluctuations in north-central Spain
¹³⁷ were more responsive to high-frequency fluctuations of drought occurring during
¹³⁸ last 15 years of the analysis. On the other hand, the tree-growth fluctuations of
¹³⁹ east Spain were responsive to middle-to-low frequency fluctuations that occurred
¹⁴⁰ during the all recorded years.

¹⁴¹ In north-central Spain, the **TRW-SPI** cross-spectrum indicated that main
¹⁴² correlations in the two time series was in the 2-4 period bands (Fig. 6). The
¹⁴³ relationship

¹⁴⁴ In north-central Spain, cross-coherences between **TRW** and **SPI** were higher
¹⁴⁵ in low-to-middle-period fluctuations occurring principally after 1998 (Fig. 6,
¹⁴⁶ upper-contour plot).

¹⁴⁷ In east Spain, **TRW** and **SPI** cross-coherences were higher in high-period
¹⁴⁸ fluctuations along the recorded years (Fig. 6, lower-contour plot) and in low-
¹⁴⁹ to-middle-period fluctuations occurring after 1995.

150 **4. References**

- 151 Bivand, R., Keitt, T., Rowlingson, B., 2015. rgdal: Bindings for the Geospatial
152 Data Abstraction Library. URL: <https://CRAN.R-project.org/package=rgdal>. r package version 1.1-1.
- 154 Bogino, S.M., Bravo, F., 2008. Growth response of *Pinus pinaster* ait.
155 to climatic variables in central spanish forests. Ann. For. Sci. 65, 1–13.
156 doi:[10.1051/forest:2008025](https://doi.org/10.1051/forest:2008025).
- 157 Bunn, A.G., 2010. Statistical and visual crossdating in r using the dplr library.
158 Dendrochronologia 28, 251 – 258. doi:[10.1016/j.dendro.2009.12.001](https://doi.org/10.1016/j.dendro.2009.12.001).
- 159 Cazelles, B., Chavez, M., Berteaux, D., Ménard, F., Vik, J.O., Jenouvrier, S.,
160 Stenseth, N.C., 2008. Wavelet analysis of ecological time series. Oecologia
161 156, 287–304. doi:[10.1007/s00442-008-0993-2](https://doi.org/10.1007/s00442-008-0993-2).
- 162 Herrera, S., Fernández, J., Gutiérrez, J., 2015. Update of the Spain02 gridded
163 observational dataset for EURO-CORDEX evaluation: assessing the effect of
164 the interpolation methodology. International Journal of Climatology .
- 165 Hijmans, R.J., 2015. raster: Geographic data analysis and modeling. URL:
166 <https://CRAN.R-project.org/package=raster>. r package version 2.4-30.
- 167 Lara, W., Bravo, F., Sierra, C., 2015. measuRing: An R package to measure
168 tree-ring widths from scanned images. Dendrochronologia 34, 43 – 50. doi:[10.1016/j.dendro.2015.04.002](https://doi.org/10.1016/j.dendro.2015.04.002).

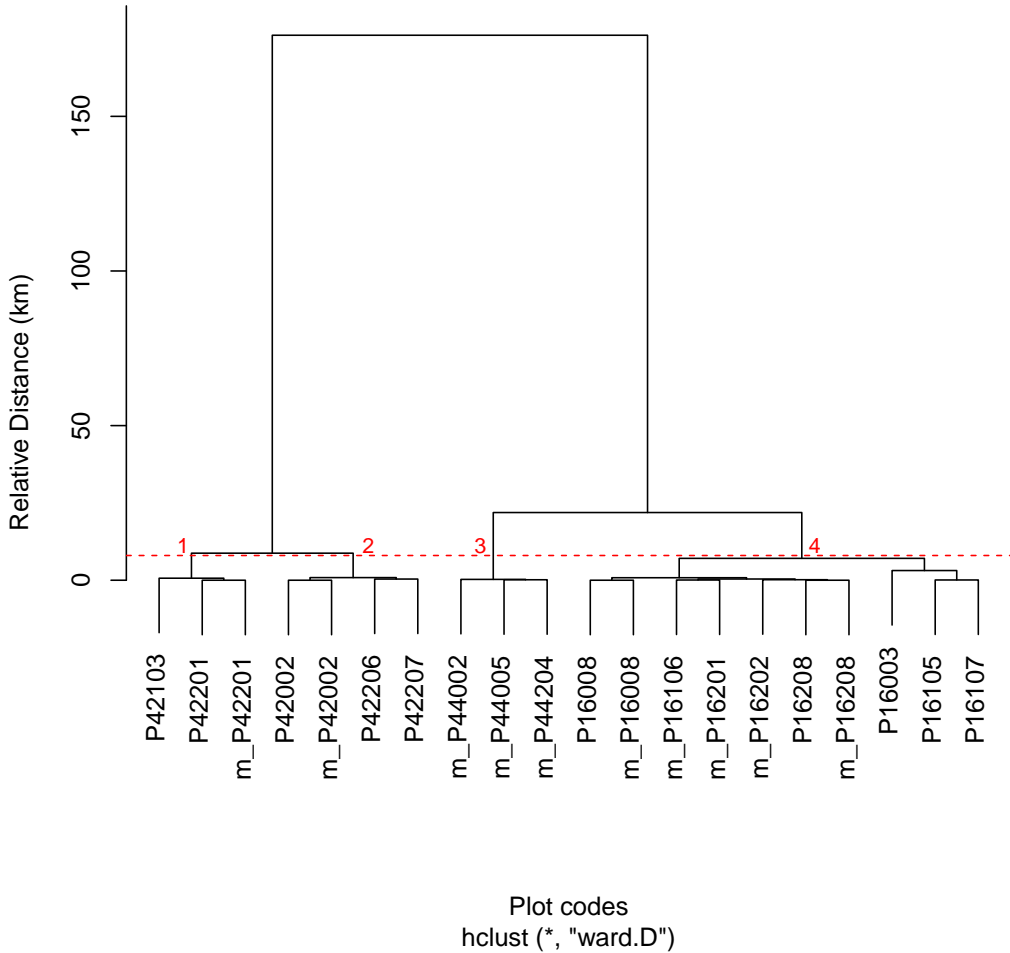


Figure 1: Geographic closeness among Tree-ring Width (TRW) chronologies of *Pinus Pinaster* Ait. (*P. pinaster*). Master chronologies are indicated with m_. Codes of the chronologies begin with initial letter of the species. The following two digits in the codes indicate spanish provinces: 42 (*Soria*) and 44 (*teruel*) in north-central Spain, and 16 (*Cuenca*) in eastern Spain. The last three digits in the codes are plot labels. Red dashed line and red numbers define four within-group cross-dating chronologies (< 8 km of cossenes)

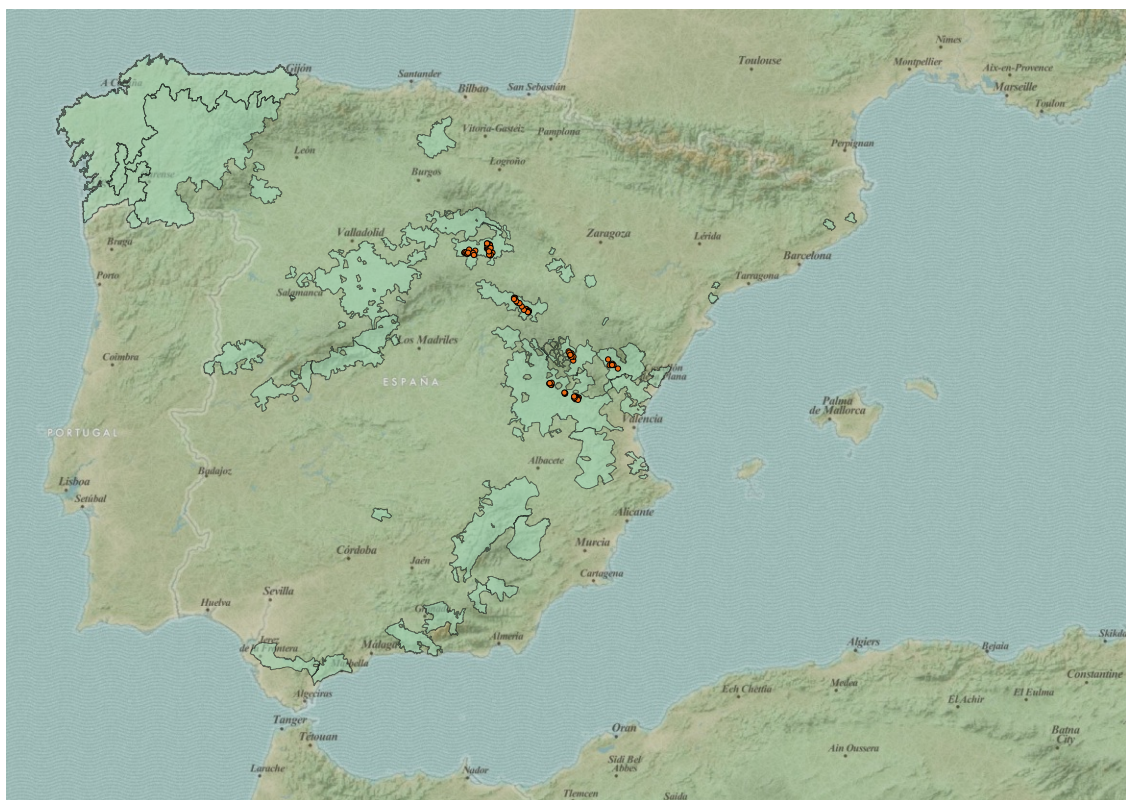


Figure 2: Study site. The green areas represent distribution of *P. pinaster* trees along Spain. The orange points represent locations of tree-ring chronologies.

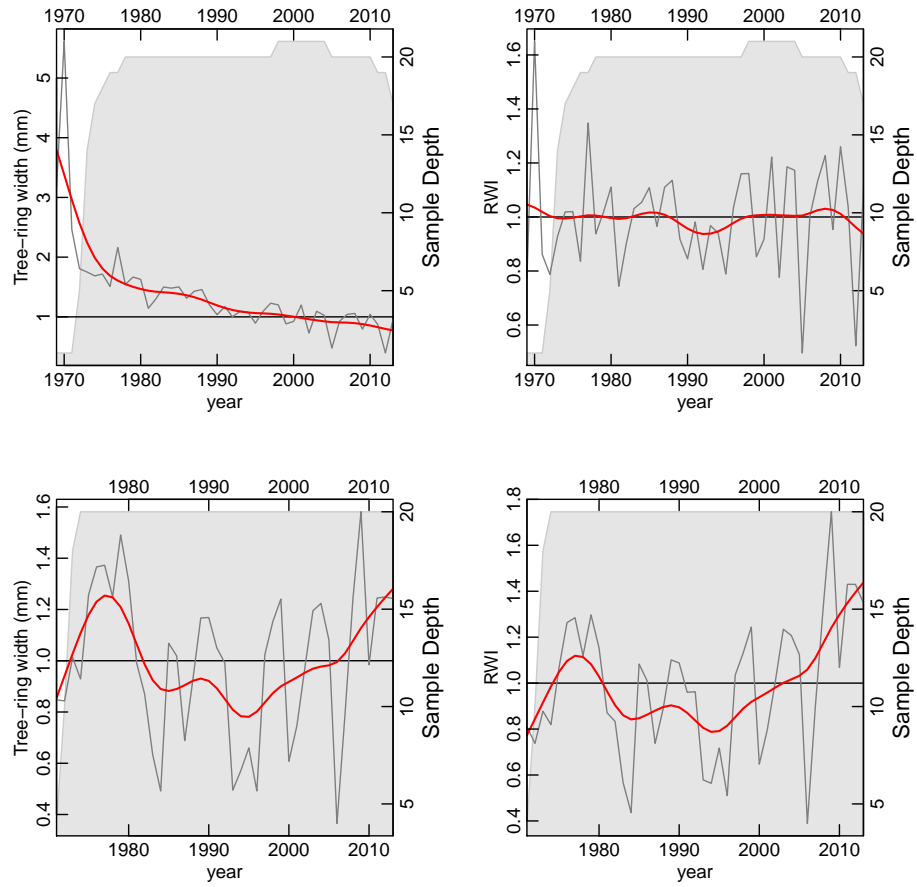


Figure 3: TRW chronologies of *P. pinaster* trees in north-central Spain (upper-panel plots) and eastern Spain (lower-panel plots). Original chronologies (left-panel plots) are detrended (right-panel plots). Gray lines are the fluctuations, and red lines (smoothing splines) are average patterns. Sample depth is the number of series available in each year.

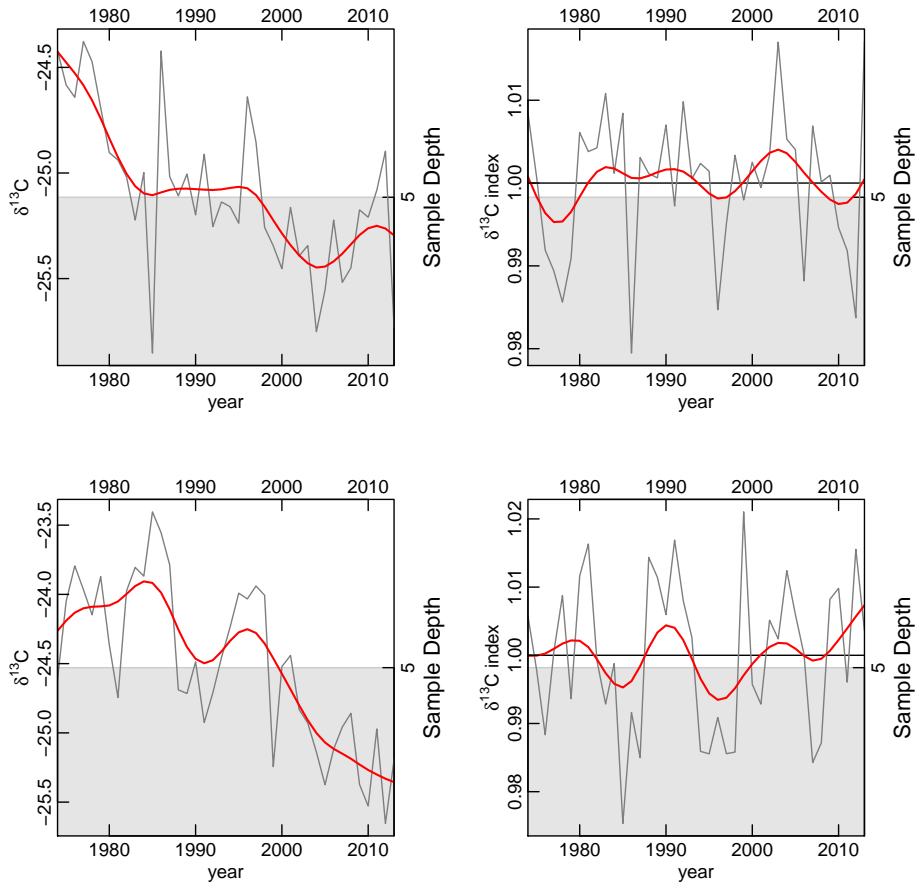


Figure 4: Late-Wood Stable $\delta^{13}\text{C}$ chronologies of *P. pinaster* trees growing on north-central Spain (upper-panel plots) and eastern Spain (lower-panel plots). Trends in the original chronologies (left-panel plots) are subtracted (right-panel plots). Gray lines are fluctuations and red lines (smoothing splines) are average patterns. Sample depth is the number of series available in each year.

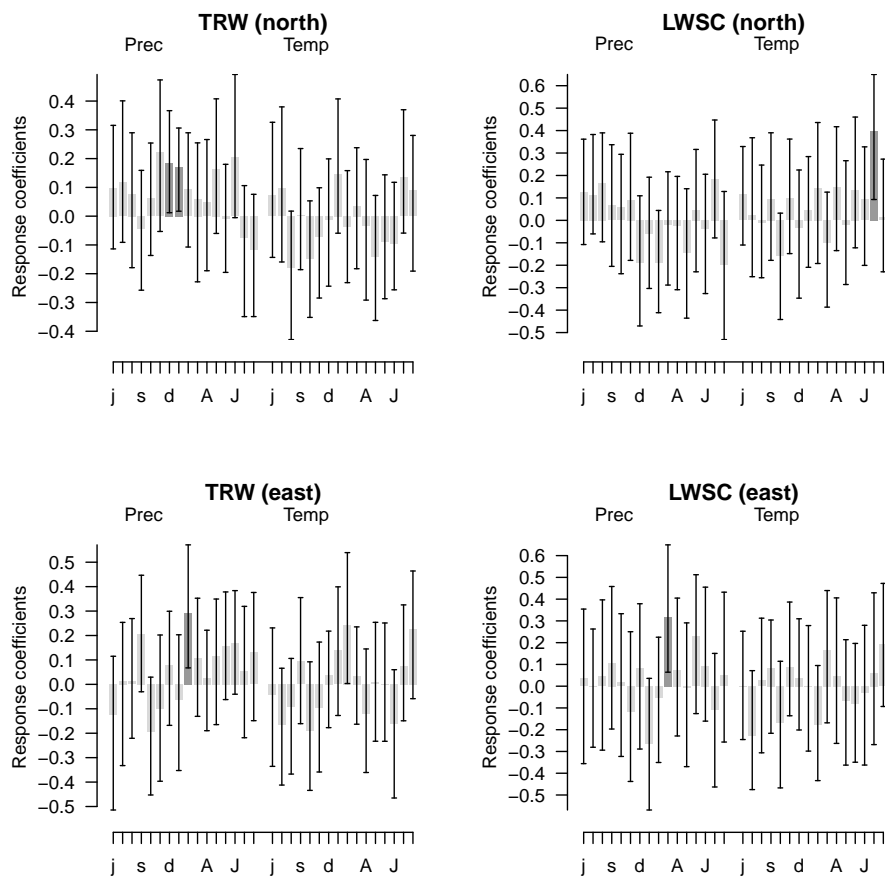


Figure 5: Intra-annual response coefficients for precipitation and temperature for Tree-ring Width (TRW) and Late-Wood Stable $\delta^{13}\text{C}$ (LWSC) chronologies of *P. pinaster*. The darker bars indicate significant coefficients ($P \leq 0.05$), and the lines represent 95%-confidence intervals.

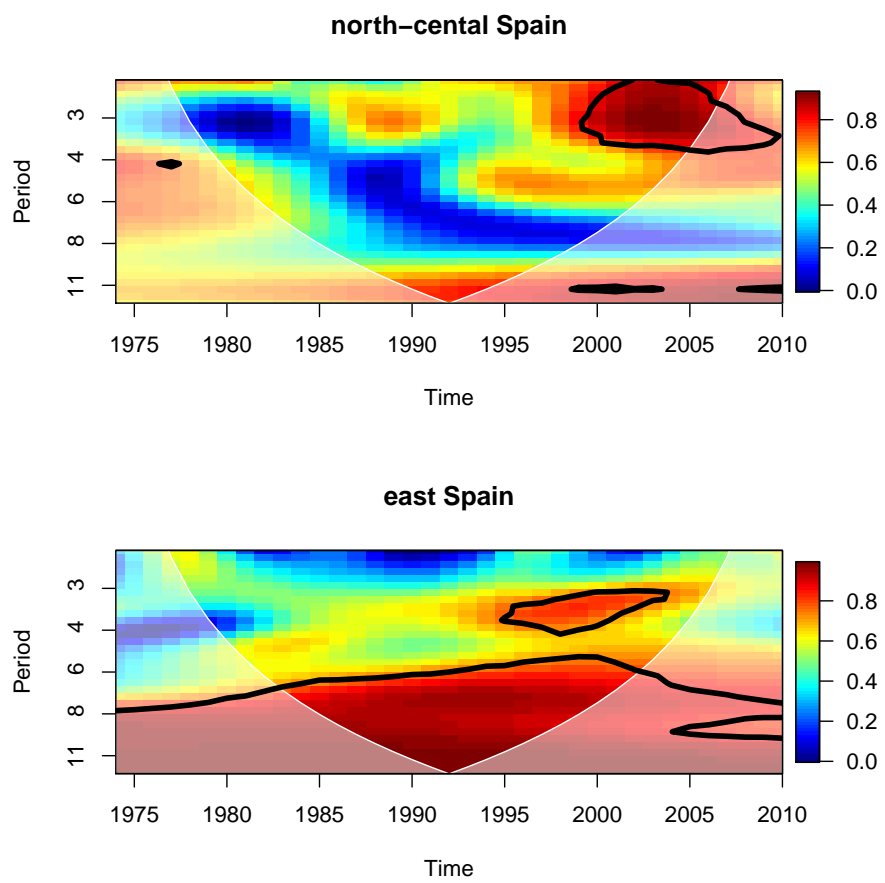


Figure 6: Wavelet coherency between signals of tree-ring widths and standardized precipitation indexes. The colored scale indicate the correlation between the two time series.